RSC Advances

PAPER

View Article Online
View Journal | View Issue

Cite this: *RSC Adv.*, 2018, **8**, 39307

Novel far-red-emitting $SrGdAlO_4:Mn^{4+}$ phosphors with excellent responsiveness to phytochrome P_{FR} for plant growth lighting

Qi Sun,[a] Shaoying Wang,[a] Balaji Devakumar,[a] Bin Li,[a] Liangling Sun,[a] Jia Liang,[a] Daqin Chen *[b] and Xiaoyong Huang *[a]

Received 16th October 2018
Accepted 19th November 2018

DOI: 10.1039/c8ra08551j

rsc.li/rsc-advances

In this work, we reported on novel far-red-emitting $SrGdAlO_4:Mn^{4+}$ (SGA:Mn^{4+}) phosphors towards application in plant growth lighting. The crystal structure and luminescence properties were investigated on the basis of X-ray diffraction, excitation and emission spectra, luminescence decay curves and temperature-dependent photoluminescence spectra. When excited by 353 nm, the SGA:Mn^{4+} phosphors showed a far-red emission band in the 650–800 nm wavelength range with peaks at 709 and 725 nm, which was due to the $^2E_g \rightarrow {}^4A_{2g}$ electron transition of Mn^{4+} ion. The optimal Mn^{4+} doping concentration was about 0.1 mol%. The CIE chromaticity coordinates of the SGA:0.1%Mn^{4+} sample were (0.7064, 0.2934). The luminescence decay lifetimes decreased gradually from 1.263 to 0.868 ms with the increasing Mn^{4+} concentrations. Notably, the emission band of SGA:0.1%Mn^{4+} sample was well-matched with the absorption spectrum of phytochrome P_{FR}, which indicated the SGA:Mn^{4+} were potential far-red-emitting phosphors for plant growth applications.

1. Introduction

In agricultural production, the lighting conditions are directly related to the success of agricultural production.[1,2] With the development of modern agriculture, the demand and energy consumption of plant lighting are expanding.[3] Using light-emitting diodes (LEDs) as artificial light sources has become an inevitable choice for agricultural development.[4] In recent years, compared with conventional light sources including fluorescent and incandescent lamps, LEDs are considered as next-generation lighting sources and thus have been receiving considerable attention owing to their tremendous merits such as short response time, long lifetimes, energy saving, low cost, and reliability.[5–14] Especially, the wavelengths of LEDs can be adjusted by using various phosphors to match with the spectral range of plant photosynthesis and photomorphogenesis, which could affect the plant growth and development by regulating phytochrome.[15,16] It is known that different wavelengths of light have different effects on plant photosynthesis, of which blue around 450 nm (410–500 nm), red light around 660 nm (610–700 nm) and far-red light around 730 nm (700–740 nm) have the greatest impact on photosynthesis.[17,18] Far-red light can be absorbed by phytochrome P_{FR} to regulate the time of flowering and the process of the plant germination.[19,20] Therefore, it is imperative to search for novel far-red phosphors with preferable luminescence performance.

Currently, Eu^{2+}-doped nitride-based red phosphors such as $CaAlSiN_3:Eu^{2+}$ have been widely reported.[21–23] However, the preparation of nitrides requires high temperature and high pressure, which leads to high synthesis cost. It is worth noting that because of their low cost and desirable spectral features, Mn^{4+}-activated red phosphors have the potential to replace Eu^{2+} based nitrides.[24–35] Compared with the Mn^{4+}-doped fluorides, Mn^{4+}-activated oxides generally show intense far-red emissions in the 650–800 nm wavelength range, which are more suitable for plant growth lighting.[36–38] The materials of Mn^{4+}-doped aluminates phosphors are cheaper than Mn^{4+}-doped germinates phosphors. Recently, Mn^{4+}-doped aluminates phosphors with eco-friendly preparation process and high chemical stability have been extensively investigated, such as $SrMgAl_{10}O_{17}:Mn^{4+}$, $Ca_{14}Al_{10}Zn_6O_{35}:Mn^{4+}$, and $CaMg_2Al_{16}O_{27}:Mn^{4+}$.[39–41] When Mn^{4+} ions substitute for Al^{3+} ions in the $[AlO_6]$ octahedral sites owing to the similar ionic radii of Al^{3+} ions and Mn^{4+} ions,[42] the phosphors would give rise to red emissions.[43,44] Up to date, the luminescence properties of Mn^{4+}-doped $SrGdAlO_4$ phosphors have never been reported. The $SrGdAlO_4$ (SGA) compound consists of many $[AlO_6]$ octahedrons and can be synthesized easily with cheap materials. Thus SGA is selected as a host for investigating the luminescence properties of Mn^{4+} and red emissions would be expected in Mn^{4+}-activated SGA phosphors.

In this paper, we reported on Mn^{4+}-doped SGA far-red-emitting phosphors prepared by a conventional high-

[a]College of Physics and Optoelectronics, Taiyuan University of Technology, Taiyuan 030024, P. R. China. E-mail: huangxy04@126.com

[b]College of Physics and Energy, Fujian Normal University, Fuzhou, Fujian 350117, P. R. China. E-mail: dqchen@fjnu.edu.cn

temperature solid-state reaction method. The crystal structure and luminescence properties of SGA:Mn^{4+} phosphors were characterized by X-ray diffraction, excitation and emission spectra, decay lifetimes, and the temperature-dependent PL spectra were analyzed in detail. These results indicated that the SGA:Mn^{4+} phosphors were very suitable to be used as far-red-emitting materials for applications in plant growth LEDs.

2. Experimental

A series of $SrGdAl_{1-x}O_4$:xMn^{4+} (SGA:xMn^{4+}; $x = 0.05$, 0.1, 0.2, 0.4, 0.6, and 0.8 mol%) phosphors were prepared by using a high-temperature solid-state reaction method. The raw materials of $SrCO_3$ (analytical reagent, AR), Gd_2O_3 (99.99%), Al_2O_3 (AR), and $MnCO_3$ (AR) were weighed according to the stoichiometric ratio and ground in an agate mortar. After that, the mixtures were put into the crucibles and pre-heated at 600 °C for 3 h, then reground and sintered again at 1500 °C for 6 h. After cooling down to room temperature naturally, the final obtained products were ground again into fine powders for subsequent characterization.

The X-ray diffraction (XRD) patterns of the samples were recorded on a Bruker D8 X-ray diffractometer with Cu Kα radiation ($\lambda = 1.5406$ Å). The photoluminescence (PL) and PL excitation (PLE) spectra and decay curves of as-obtained phosphors were measured using an Edinburgh FS5 spectrometer equipped with a 150 W continued-wavelength xenon lamp and a pulsed xenon lamp, respectively. Furthermore, the temperature-dependent PL spectra of the phosphors were obtained from the same instrument attached a temperature controlling system. The internal quantum efficiency (IQE) was measured by an Edinburgh FS5 spectrometer equipped with an integrating sphere coated with $BaSO_4$.

3. Results and discussion

Fig. 1 shows the XRD patterns of SGA:xMn^{4+} ($x = 0.1\%$, 0.4%, and 0.8%) phosphors. It was found that all the observed diffraction peaks were consistent with the standard JCPDS card of SGA (no. 24-1185), demonstrating that Mn^{4+} ions were well-doped into the host and there was no significant influence on the structure of SGA.

Fig. 2 shows the typical crystal structure of SGA. The SGA compound belonged to tetragonal crystal system with space group *I*4/*mmm*. The lattice constants were determined to be $a = b = 3.697$ Å, $c = 12.360$ Å, $V = 168.9$ Å^3, and $\alpha = \beta = \gamma = 90°$. It was obvious that Gd^{3+} and Sr^{2+} ions were coordinated with nine oxygen atoms around them, and the Al^{3+} ions were coordinated by six oxygen atoms to form [AlO_6] octahedrons. Because of the similar ionic radii of Al^{3+} ($r = 0.535$ Å, coordination number (CN) = 6) and Mn^{4+} ($r = 0.530$ Å, CN = 6) ions, Mn^{4+} ions tended to replace Al^{3+} ions sites in SGA:Mn^{4+} phosphors.[45]

Fig. 3(a) shows the PLE and PL spectra of SGA:0.1%Mn^{4+} sample at room temperature. When monitored at 709 nm, the obtained PLE spectrum of SGA:0.1%Mn^{4+} sample included two wide excitation bands peaking at 353 and 490 nm in the wavelength range from 250 to 600 nm, which were assigned to the

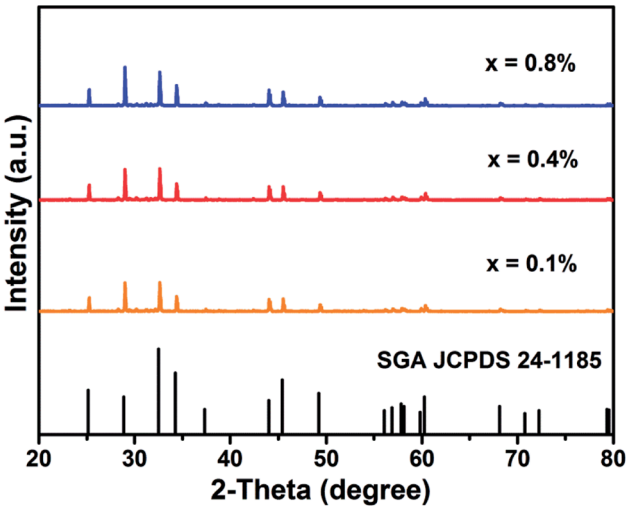

Fig. 1 XRD patterns of SGA:xMn^{4+} ($x = 0.1\%$, 0.4%, and 0.8%) phosphors and the standard profile of SGA (JCPDS no. 24-1185).

Mn^{4+} spin-allowed transitions of $^4A_{2g} \rightarrow {}^4T_{1g}$ and $^4A_{2g} \rightarrow {}^4T_{2g}$, respectively.[46–48] The two broad bands in the PLE spectrum indicated that the SGA:Mn^{4+} phosphors could be excited by both ultraviolet (UV) and blue LED chips. When excited at 353 nm, the SGA:0.1%Mn^{4+} sample emitted bright far-red light. The PL spectrum consisted of a far-red emission band in the wavelength range of 650–800 nm with two sharp peaks at 709 and 725 nm, which was due to the spin-forbidden $^2E_g \rightarrow {}^4A_{2g}$

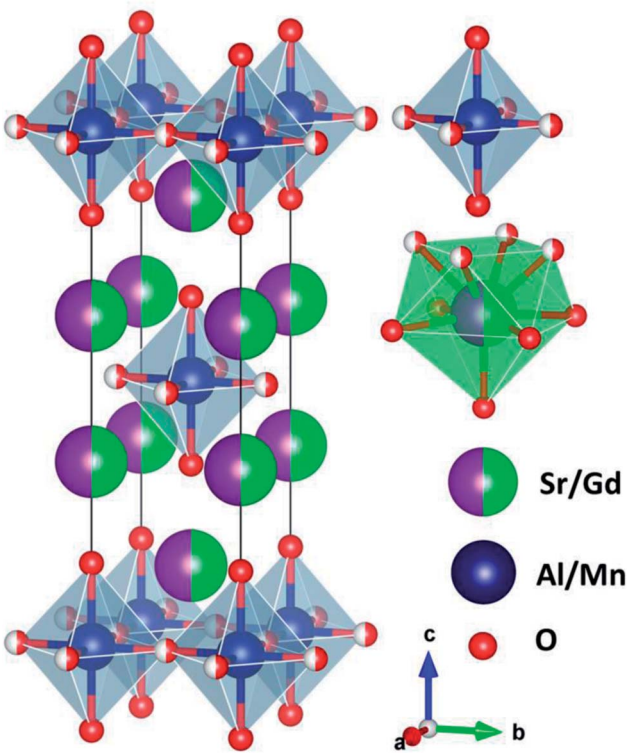

Fig. 2 Typical crystal structure of SGA and the Al^{3+} and Sr^{2+}/Gd^{3+} sites are coordinated by six and nine oxygen atoms, respectively.

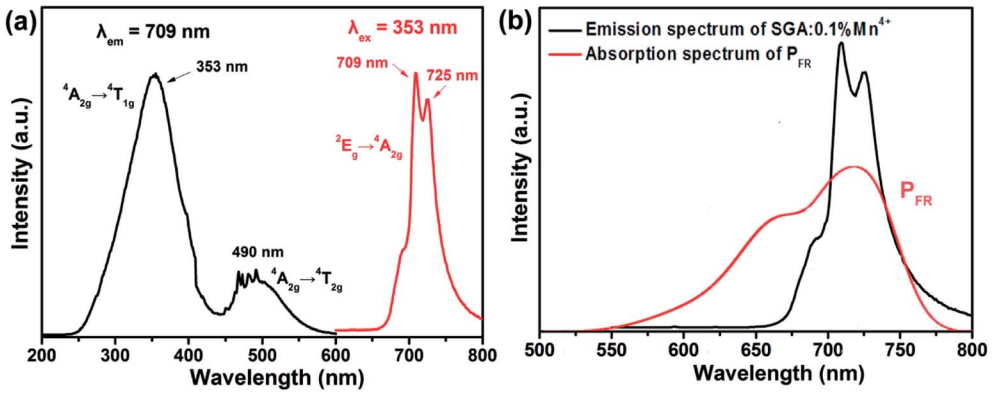

Fig. 3 (a) PLE and PL spectra of SGA:0.1%Mn^{4+} phosphors. (b) PL spectrum of SGA:0.1%Mn^{4+} phosphors and the absorption spectrum of phytochrome P_{FR}.

transition of Mn^{4+}.[49–52] Fig. 3(b) compares the PL spectrum of SGA:0.1%Mn^{4+} phosphors and the absorption spectrum of phytochrome P_{FR}. Obviously, there was an significant spectral overlap between the emission band of SGA:0.1%Mn^{4+} phosphors and the absorption of phytochrome P_{FR}, implying that the SGA:Mn^{4+} phosphors could be potential far-red-emitting phosphors used in plant growth LEDs applications to promote plant development.[53]

To determine the optimal Mn^{4+} doping concentration, the PL spectra of SGA:Mn^{4+} phosphors with different Mn^{4+} doping concentrations under 353 nm excitation were measured, as displayed in Fig. 4(a). The shapes and positions of the PL spectra of SGA:Mn^{4+} doped with various Mn^{4+} contents were very similar, but the emission intensities varied. As depicted in Fig. 4(b), when the Mn^{4+} doping concentration increased, the emission intensity of SGA:$x$$Mn^{4+}$ phosphors increased first and reached a maximum value at $x = 0.1\%$, then decreased gradually with further increase in the Mn^{4+} concentrations. This phenomenon was attributed to concentration quenching effect, which was caused by the energy migration between neighboring Mn^{4+} activators.[54,55] Because no spectral overlap was observed between PLE and PL spectra of SGA:Mn^{4+}, so the radiation reabsorption was not the mechanism responsible for concentration quenching effect. If the distance between Mn^{4+} ions is higher than 5 Å, electric multipolar interaction is the dominant mechanism for concentration quenching effect; otherwise, exchange interaction becomes main mechanism for the concentration quenching.[56,57] In order to investigate which mechanism was primary for the concentration quenching among the nearest Mn^{4+} ions of the SGA host, the critical distance (R_c) was roughly calculated using the following equation:[58]

$$R_c \approx 2\left[\frac{3V}{4\pi X_c N}\right]^{1/3}, \quad (1)$$

where V is the volume of the unit cell, X_c stands for the critical doping concentration of Mn^{4+} ions, and N represents the number of available sites for the dopant in the unit cell. For the SGA host, the $X_c = 0.1\%$; $V = 168.9$ Å^3; and $N = 2$. The calculated R_c value was 54.43 Å, which was larger than 5 Å. Thus, the concentration quenching effect in the SGA:Mn^{4+} phosphors was mainly caused *via* electric multipolar interactions. Moreover, we can use the following equation to confirm the type of interaction mechanism among Mn^{4+} ions:[58]

$$I/x = K[1 + \beta(x)^{\theta/3}]^{-1}, \quad (2)$$

where I and x are the PL intensity and doping concentration of Mn^{4+} ions in SGA host, respectively; β and K are constants; and θ represents an index of the electric multipolar character, where $\theta = 6$, 8 and 10 corresponding to dipole–dipole, dipole–quadrupole and quadrupole–quadrupole interactions, respectively.[59,60] Fig. 4(c) shows the plot of $\log(I/x)$ *versus* $\log(x)$. The slope $(-\theta/3)$ of the fitted line was found to be -1.487, and thus the value of θ was 4.461, which was close to 3. Therefore, the concentration quenching mechanism was the non-radiative energy transfer among the adjacent Mn^{4+} ions in SGA:Mn^{4+} phosphors, which was similar to the previous research.[53,61–63]

Fig. 5 illustrates the CIE chromaticity diagram of SGA:0.1%Mn^{4+} sample. According to its PL spectrum, the CIE chromaticity coordinates were calculated to be (0.7064, 0.2934), which were located in the far-red region. The color purity of SGA:0.1%Mn^{4+} sample was calculated to be 93%. As shown in the inset of Fig. 5, the SGA:0.1%Mn^{4+} sample emitted bright red light under 365 nm UV lamp. Therefore, the SGA:Mn^{4+} phosphors can be developed as potential far-red-emitting phosphors for applications in plant growth.

Fig. 6 shows PL decay curves of SGA:$x$$Mn^{4+}$ ($x = 0.05\%$, 0.1%, 0.2%, 0.4%, 0.6%, and 0.8%) samples monitored at 709 nm and excited at 353 nm. All the decay curves could be well-fitted by the following equation:[48]

$$I_t = A_1 \exp\left(-\frac{t}{\tau_1}\right) + A_2 \exp\left(-\frac{t}{\tau_2}\right) \quad (3)$$

where I_t is the luminescence intensities of SGA:$x$$Mn^{4+}$ phosphors at time t, A_1 and A_2 represent constants, and τ_1 and τ_2 correspond to the short and long lifetimes for the exponential components, respectively. Furthermore, the average lifetime τ_s could be calculated by the following equation:[48]

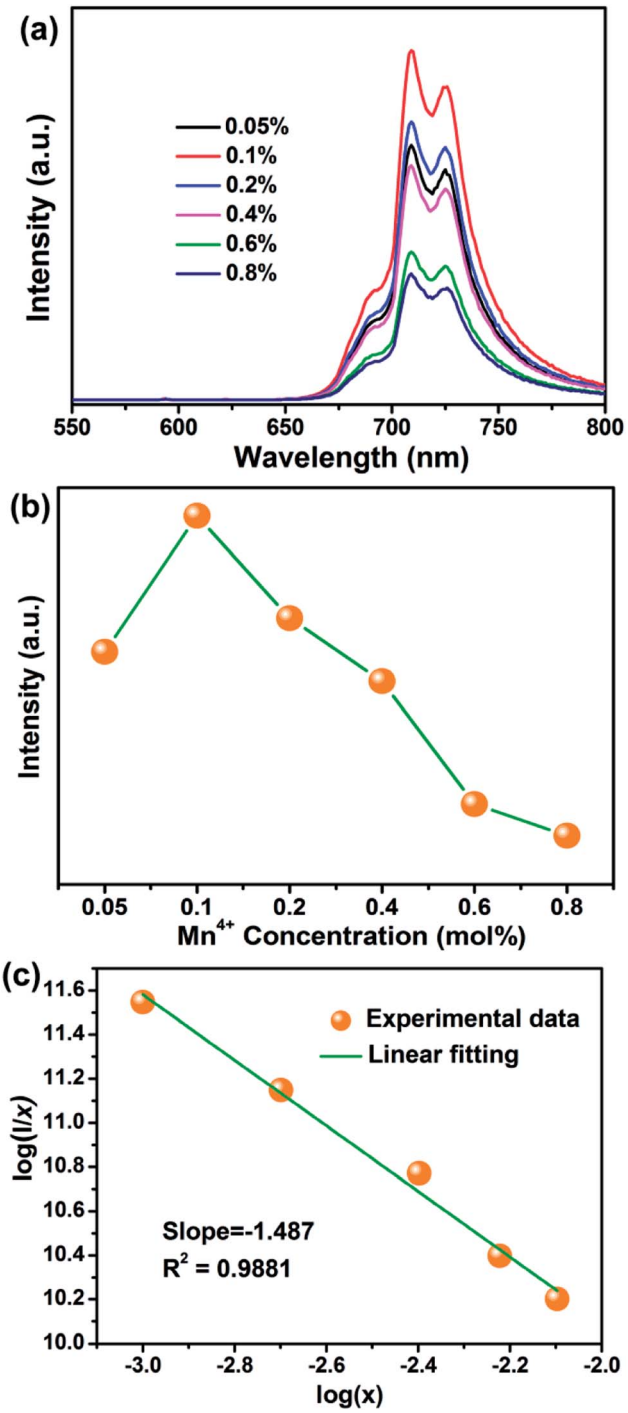

Fig. 4 (a) PL spectra of SGA:xMn^{4+} (x = 0.05%, 0.1%, 0.2%, 0.4%, 0.6%, and 0.8%) phosphors under 353 nm excitation. (b) PL intensity of SGA:xMn^{4+} as a function of Mn^{4+} doping concentrations. (c) Linear fitting of log(x) *versus* log(I/x) in SGA:xMn^{4+} phosphors excited at 353 nm.

$$\tau_s = (A_1\tau_1^2 + A_2\tau_2^2)/(A_1\tau_1 + A_2\tau_2) \quad (4)$$

The decay times values were calculated and shown in Fig. 6. It was worth noting that the decay times of SGA:xMn^{4+} samples gradually decreased with increasing Mn^{4+} doping concentrations. The results was caused by the reduced distance between Mn^{4+}–Mn^{4+} pairs in the host as high Mn^{4+} concentrations were doped, and then non-radiative transition rate increased among Mn^{4+} ions and finally the lifetimes of samples were decreased.[64]

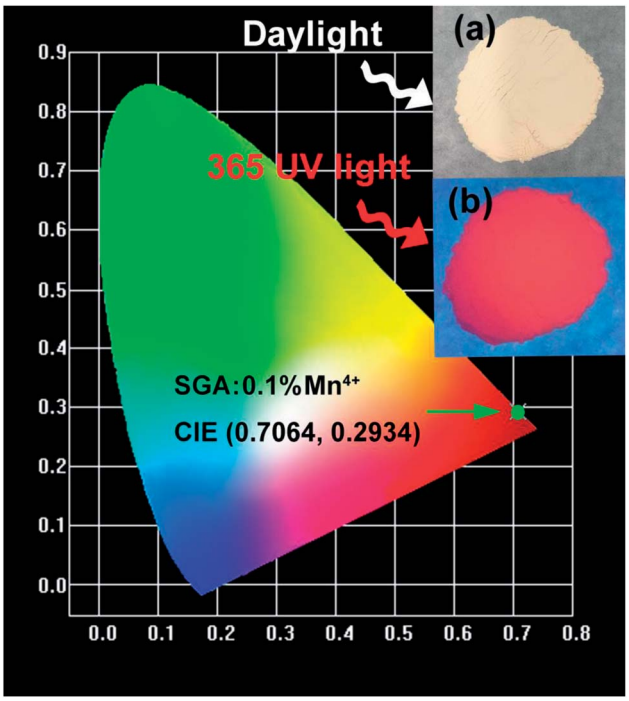

Fig. 5 CIE chromaticity coordinates of SGA:0.1%Mn^{4+} phosphors under 353 nm excitation. The inset shows the digital photographs of SGA:0.1%Mn^{4+} phosphors in daylight and under a 365 nm UV lamp.

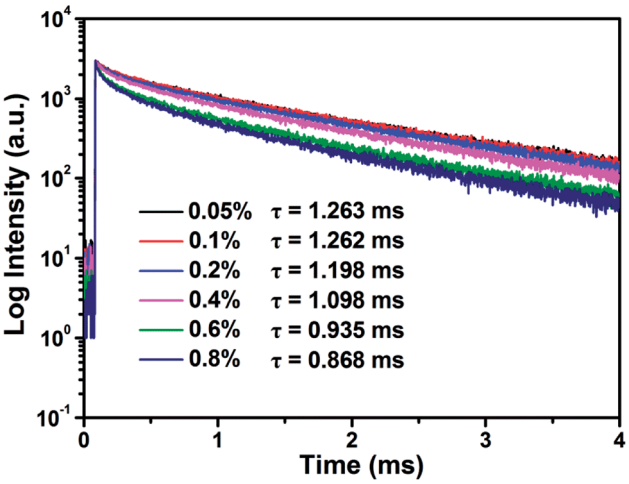

Fig. 6 Decay curves and calculated lifetimes of SGA:xMn^{4+} (x = 0.05%, 0.1%, 0.2%, 0.4%, 0.6%, and 0.8%) under 353 nm excitation and monitored at 709 nm.

Fig. 7(a) shows the temperature-dependent emission spectra of SGA:0.1%Mn^{4+} sample measured in the temperature range of 303 K to 463 K. With the excitation at 353 nm, it was obvious that there was no significant distinction among the emission

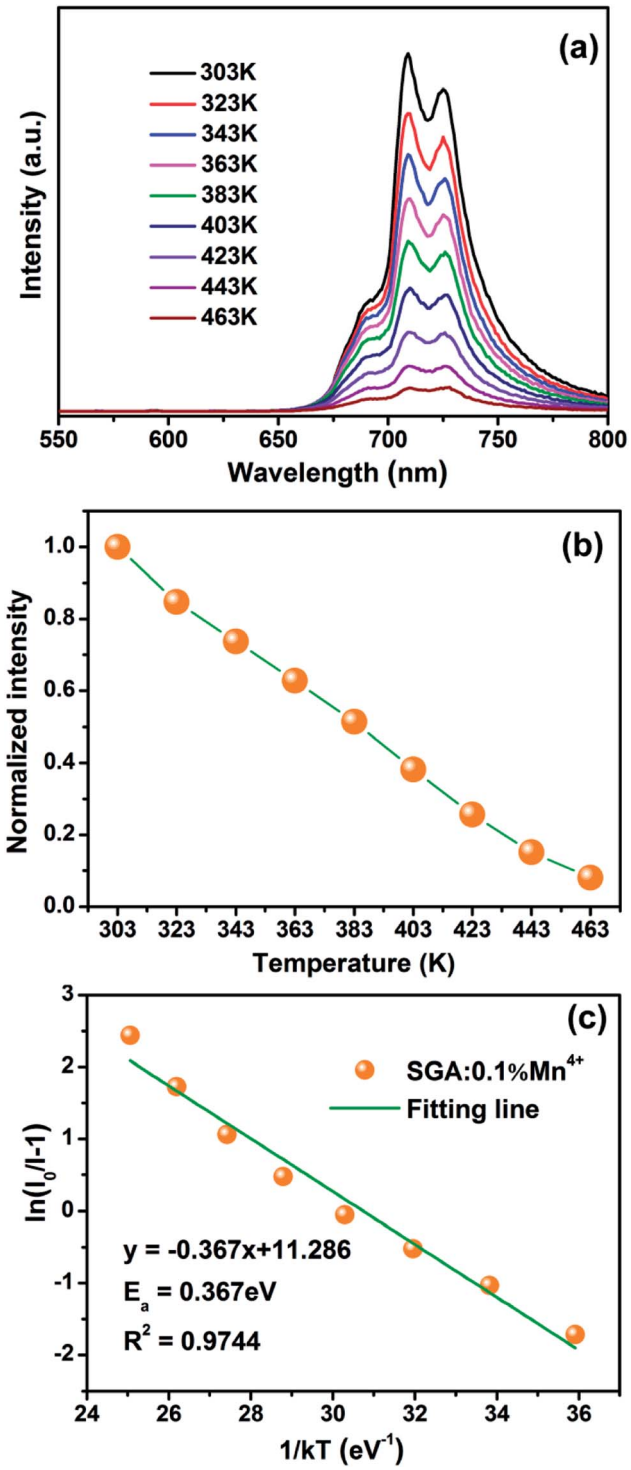

Fig. 7 (a) Temperature-dependent PL spectra of SGA:0.1%Mn^{4+} phosphors under 353 nm excitation. (b) The normalized PL intensities of SGA:0.1%Mn^{4+} phosphors at different temperature from 303 to 463 K. (c) The plot of $\ln(I_0/I - 1)$ *versus* $1/kT$.

spectra. However, the PL intensity of SGA:0.1%Mn^{4+} sample gradually decreased with increasing temperature, which was due to thermal quenching.[65] Fig. 7(b) shows the normalized PL intensity as a function of temperature. It was found that the intensity of the sample decreased to ~50% of the initial emission intensity when the temperature at 383 K (110 °C). The value of activation energy E_a was crucial for thermal quenching effect, which could be evaluated using the equation as follows:[66]

$$\ln\left(\frac{I_0}{I} - 1\right) = \ln A - \frac{E_a}{kT}, \quad (5)$$

where I_0 and I are the emission intensity of the SGA:0.1%Mn^{4+} phosphor at initial temperature and at different given temperatures T, respectively; k stands for the Boltzmann constant; A is the constant; and E_a represents activation energy. According to the equation, the fitted linear relationship between $\ln(I_0/I - 1)$ and $1/kT$ was given in Fig. 7(c). Thus, the value of E_a was determined to be 0.367 eV. Furthermore, the IQE value of SGA:0.1%Mn^{4+} phosphors was 23%, which was higher than several other Mn^{4+} doped oxides, such as $Ca_{14}Al_{10}Zn_6O_{35}$:Mn^{4+} (IQE: 19.4%),[2] and $Na_2MgAl_{10}O_{17}$:Mn^{4+} (IQE: 22.7%).[67]

4. Conclusions

In conclusion, a novel series of far-red-emitting SGA:Mn^{4+} phosphors were synthesized by a conventional high-temperature solid-state reaction method. The phosphors could be efficiently excited by both UV and blue LED chips and showed far-red emission between 650 and 800 nm peaking at 709 nm and 725 nm. The emission band of the SGA:Mn^{4+} phosphors was matched well with the absorption spectrum of phytochrome P_{FR}. The optimal Mn^{4+} doping concentration was about 0.1 mol% and the corresponding CIE chromaticity coordinates were (0.7064, 0.2934). The concentration quenching mechanism was the non-radiative energy transfer among the adjacent Mn^{4+} ions in SGA:Mn^{4+} phosphors. Moreover, the value of E_a was determined to be 0.367 eV. All above results proved that the SGA:Mn^{4+} phosphors could emit brilliant far-red light for applications in plant growth.

Conflicts of interest

There are no conflicts to declare.

Acknowledgements

This work was supported by the National Natural Science Foundation of China (No. 51502190), the Program for the Outstanding Innovative Teams of Higher Learning Institutions of Shanxi, and the Open Fund of the State Key Laboratory of Luminescent Materials and Devices (South China University of Technology, No. 2017-skllmd-01).

References

1 Z. Zhou, M. Xia, Y. Zhong, S. Gai, S. Huang, Y. Tian, X. Lu and N. Zhou, *J. Mater. Chem. C*, 2017, **5**, 8201–8210.
2 L. Li, Y. Pan, Z. Chen, S. Huang and M. Wu, *RSC Adv.*, 2017, **7**, 14868–14875.
3 J. Deng, H. Zhang, X. Zhang, Y. Zheng, J. Yuan, H. Liu, Y. Liu, B. Lei and J. Qiu, *J. Mater. Chem. C*, 2018, **6**, 1738–1745.

4 J. Long, X. Yuan, C. Ma, M. Du, X. Ma, Z. Wen, R. Ma, Y. Wang and Y. Cao, *RSC Adv.*, 2018, **8**, 1469–1476.
5 X. Huang, *J. Alloys Compd.*, 2017, **690**, 356–359.
6 X. Huang, H. Guo and B. Li, *J. Alloys Compd.*, 2017, **720**, 29–38.
7 X. Huang, B. Li and H. Guo, *Ceram. Int.*, 2017, **43**, 10566–10571.
8 X. Huang, B. Li and H. Guo, *J. Alloys Compd.*, 2017, **695**, 2773–2780.
9 X. Huang, B. Li, H. Guo and D. Chen, *Dyes Pigm.*, 2017, **143**, 86–94.
10 X. Huang, S. Wang, B. Li, Q. Sun and H. Guo, *Opt. Lett.*, 2018, **43**, 1307–1310.
11 B. Li, X. Huang, H. Guo and Y. Zeng, *Dyes Pigm.*, 2018, **150**, 67–72.
12 X. Huang and H. Guo, *Dyes Pigm.*, 2018, **154**, 82–86.
13 B. Li, G. Annadurai, L. Sun, J. Liang, S. Wang, Q. Sun and X. Huang, *Opt. Lett.*, 2018, **43**, 5138–5141.
14 H. Guo, B. Devakumar, B. Li and X. Huang, *Dyes Pigm.*, 2018, **151**, 81–88.
15 J. Xiang, J. Chen, N. Zhang, H. Yao and C. Guo, *Dyes Pigm.*, 2018, **154**, 257–262.
16 R. Cao, Z. Shi, G. Quan, T. Chen, S. Guo, Z. Hu and P. Liu, *J. Lumin.*, 2017, **188**, 577–581.
17 Q. Sun, S. Wang, B. Li, H. Guo and X. Huang, *J. Lumin.*, 2018, **203**, 371–375.
18 Z. Zhou, J. Zheng, R. Shi, N. Zhang, J. Chen, R. Zhang, H. Suo, E. M. Goldys and C. Guo, *ACS Appl. Mater. Interfaces*, 2017, **9**, 6177–6185.
19 X. Huang, J. Liang, B. Li, L. Sun and J. Lin, *Opt. Lett.*, 2018, **43**, 3305–3308.
20 Q. Sun, S. Wang, B. Devakumar, B. Li, L. Sun, J. Liang and X. Huang, *RSC Adv.*, 2018, **8**, 28538–28545.
21 K. Uheda, N. Hirosaki, Y. Yamamoto, A. Naito, T. Nakajima and H. Yamamoto, *Electrochem. Solid-State Lett.*, 2006, **9**, H22–H25.
22 X. Huang, *Nat. Photonics*, 2014, **8**, 748–749.
23 P. Du, X. Huang and J. S. Yu, *Chem. Eng. J.*, 2018, **337**, 91–100.
24 R. Cao, X. Ceng, J. Huang, H. Ao, G. Zheng, X. Yu and X. Zhang, *Opt. Mater.*, 2016, **62**, 706–710.
25 R. Cao, X. Ceng, J. Huang, X. Xia, S. Guo and J. Fu, *Ceram. Int.*, 2016, **42**, 16817–16821.
26 R. Cao, X. Liu, K. Bai, T. Chen, S. Guo, Z. Hu, F. Xiao and Z. Luo, *J. Lumin.*, 2018, **197**, 169–174.
27 R. Cao, Z. Shi, G. Quan, Z. Luo, P. Tang, H. Ao and X. Yu, *Opt. Mater.*, 2016, **57**, 212–216.
28 R. Cao, W. Wang, J. Zhang, S. Jiang, Z. Chen, W. Li and X. Yu, *J. Alloys Compd.*, 2017, **704**, 124–130.
29 R. Cao, J. Zhang, W. Wang, T. Chen, Q. Gou, Y. Wen, F. Xiao and Z. Luo, *Opt. Mater.*, 2017, **66**, 293–296.
30 R. Cao, J. Zhang, W. Wang, Z. Hu, T. Chen, Y. Ye and X. Yu, *Mater. Res. Bull.*, 2017, **87**, 109–113.
31 Y. Zhu, L. Huang, R. Zou, J. Zhang, J. Yu, M. Wu, J. Wang and Q. Su, *J. Mater. Chem. C*, 2016, **4**, 5690–5695.
32 Y. Zhu, L. Cao, M. G. Brik, X. Zhang, L. Huang, T. Xuan and J. Wang, *J. Mater. Chem. C*, 2017, **5**, 6420–6426.
33 M. Zhu, Y. Pan, Y. Huang, H. Lian and J. Lin, *J. Mater. Chem. C*, 2018, **6**, 491–499.
34 S. Zhang, Y. Hu, H. Duan, L. Chen, Y. Fu, G. Ju, T. Wang and M. He, *RSC Adv.*, 2015, **5**, 90499–90507.
35 L. Qin, S. Bi, P. Cai, C. Chen, J. Wang, S. I. Kim, Y. Huang and H. J. Seo, *J. Alloys Compd.*, 2018, **755**, 61–66.
36 X. Huang and H. Guo, *Dyes Pigm.*, 2018, **152**, 36–42.
37 J. Liang, L. Sun, B. Devakumar, S. Wang, Q. Sun, H. Guo, B. Li and X. Huang, *RSC Adv.*, 2018, **8**, 27144–27151.
38 G. Jiang, B. Yang, G. Zhao, Y. Liu, J. Zou, H. Sun, H. Ou, Y. Fang and J. Hou, *Opt. Mater.*, 2018, **83**, 93–98.
39 L. Meng, L. Liang and Y. Wen, *J. Mater. Sci.: Mater. Electron.*, 2014, **25**, 2676–2681.
40 W. Lu, W. Lv, Q. Zhao, M. Jiao, B. Shao and H. You, *Inorg. Chem.*, 2014, **53**, 11985–11990.
41 B. Wang, H. Lin, J. Xu, H. Chen and Y. Wang, *ACS Appl. Mater. Interfaces*, 2014, **6**, 22905–22913.
42 D. Chen, Y. Zhou, W. Xu, J. Zhong, Z. Ji and W. Xiang, *J. Mater. Chem. C*, 2016, **4**, 1704–1712.
43 B. Wang, H. Lin, F. Huang, J. Xu, H. Chen, Z. Lin and Y. Wang, *Chem. Mater.*, 2016, **28**, 3515–3524.
44 M. Zhu, Y. Pan, L. Xi, H. Lian and J. Lin, *J. Mater. Chem. C*, 2017, **5**, 10241–10250.
45 Y. Chen, K. Wu, J. He, Z. Tang, J. Shi, Y. Xu and Z. Liu, *J. Mater. Chem. C*, 2017, **5**, 8828–8835.
46 K. Li, H. Lian and R. V. Deun, *J. Lumin.*, 2018, **198**, 155–162.
47 J. Zhong, S. Zhou, D. Chen, J. Li, Y. Zhu, X. Li, L. Chen and Z. Ji, *Dalton Trans.*, 2018, **47**, 8248–8256.
48 J. Zhong, D. Chen, X. Chen, K. Wang, X. Li, Y. Zhu and Z. Ji, *Dalton Trans.*, 2018, **47**, 6528–6537.
49 C. Yang, Z. Zhang, G. Hu, R. Cao, X. Liang and W. Xiang, *J. Alloys Compd.*, 2017, **694**, 1201–1208.
50 F. Xue, Y. Hu, L. Chen, H. Wu, G. Ju, T. Wang and L. Yang, *Ceram. Int.*, 2017, **43**, 15141–15145.
51 S. Liang, M. Shang, H. Lian, K. Li, Y. Zhang and J. Lin, *J. Mater. Chem. C*, 2016, **4**, 6409–6416.
52 S. Liang, M. Shang, H. Lian, K. Li, Y. Zhang and J. Lin, *J. Mater. Chem. C*, 2017, **5**, 2927–2935.
53 S. Wang, Q. Sun, B. Devakumar, L. Sun, J. Liang and X. Huang, *RSC Adv.*, 2018, **8**, 30191–30200.
54 S. Zhang and Y. Hu, *J. Lumin.*, 2016, **177**, 394–401.
55 X. Ding, Q. Wang and Y. Wang, *Phys. Chem. Chem. Phys.*, 2016, **18**, 8088–8097.
56 H. Guo and X. Huang, *J. Alloys Compd.*, 2018, **764**, 809–814.
57 H. Guo, X. Huang and Y. Zeng, *J. Alloys Compd.*, 2018, **741**, 300–306.
58 Y. Jin, Y. Hu, H. Wu, H. Duan, L. Chen, Y. Fu, G. Ju, Z. Mu and M. He, *Chem. Eng. J.*, 2016, **288**, 596–607.
59 A. Fu, Q. Pang, H. Yang and L. Zhou, *Opt. Mater.*, 2017, **70**, 144–152.
60 H. Chen, H. Lin, Q. Huang, F. Huang, J. Xu, B. Wang, Z. Lin, J. Zhou and Y. Wang, *J. Mater. Chem. C*, 2016, **4**, 2374–2381.
61 X. Huang and H. Guo, *RSC Adv.*, 2018, **8**, 17132–17138.
62 H. Deng, Z. Gao, N. Xue, J. H. Jeong and R. Yu, *J. Lumin.*, 2017, **192**, 684–689.
63 R. Yu, H. M. Noh, B. K. Moon, B. C. Choi, J. H. Jeong, K. Jang, S. S. Yi and J. K. Jang, *J. Alloys Compd.*, 2013, **576**, 236–241.

64 W. Chen, Y. Cheng, L. Shen, C. Shen, X. Liang and W. Xiang, *J. Alloys Compd.*, 2018, **762**, 688–696.
65 Z. Lu, A. Fu, F. Gao, X. Zhang and L. Zhou, *J. Lumin.*, 2018, **203**, 420–426.
66 Z. Liu, G. Shao, W. Chen, G. Hu, L. Shen, Y. Cheng, X. Liang and W. Xiang, *Opt. Mater. Express*, 2018, **8**, 2532–2541.
67 Q. Peng, R. Cao, Y. Ye, S. Guo, Z. Hu, T. Chen and G. Zheng, *J. Alloys Compd.*, 2017, **725**, 139–144.